JOURNAL OF SPACECRAFT AND ROCKETS
Vol. 31, No. 2, March–April 1994

Effects of Gas Models on Hypersonic Base Flow Calculations

M. S. Kim,* J. M. Loellbach,* and K. D. Lee†
University of Illinois, Urbana, Illinois 61801

Numerical solutions for the Navier-Stokes equations are obtained for laminar, hypersonic flows around a flat-based projectile using perfect gas, equilibrium air, and nonequilibrium air models. The effects of different gas models are investigated for a freestream condition of Mach 20 at an altitude of 73 km. The species compositions for the equilibrium and nonequilibrium gases are obtained by minimizing the Helmholtz free energy and by solving species continuity equations, respectively. The chemical equations are combined with the gasdynamics equations using a loosely coupled technique. A finite volume method is implemented with the flux vector splitting of Steger and Warming for convective terms and centered differencing for viscous terms. Both explicit and implicit time integration schemes are used.

Nomenclature

b_l = number of atoms in element l
C_s = mass fraction of specie s
E, H = total energy and total enthalpy
h = area of grid cell
$\tilde{h}_s$ = dimensional enthalpy of species s, J/kg
K_f, K_b = forward and backward reaction rates
$\tilde{M}_s$ = molecular weight of species s, kg/kg-mole
m = number of elements or number of chemical reactions
n = number of chemical species
n_t = number of reactants
Pr = Prandtl number
p = pressure
Re = Reynolds number per unit length, m^{-1}
$\tilde{T}$ = dimensional temperature, K
U, V = contravariant velocity components in ξ and η directions
u, v = velocity components in x and y directions
$\tilde{w}_s$ = mass production rate of species s, kg/m^{3}s
x, y = Cartesian coordinates
Z = third-body efficiency
α = speed of sound
α_{ls} = number of kg-mole of element l per kg-mole of species s
γ_s = mole-mass ratio of species s
μ = viscosity coefficient
μ_s = chemical potential of species s
$\nu_{k,s}$ = stoichiometric coefficient of species s in reaction k
ξ, η = transformed coordinates
ρ = density

Superscripts
0 = standard state
′ = forward reaction
″ = backward reaction

Introduction

HYPERSONIC vehicle design requires accurate flowfield prediction capability to improve aerodynamic efficiency, thermal protection, and propulsion system integration. A hypersonic vehicle leaves behind a long trail of hot air. The flow pattern far downstream of a hypersonic vehicle has been well established both analytically and experimentally. However, the hypersonic near-wake field immediately behind the vehicle base exhibits complex flow characteristics and requires a quantitative analysis of the flow physics. The near-wake flowfield is a transition region from the vehicle-dominated flow to the isobaric far-wake region. The far-wake region is strongly dependent on the near-wake flow conditions, so small variations in certain near-wake properties can result in large changes in far-wake characteristics. Therefore, an accurate

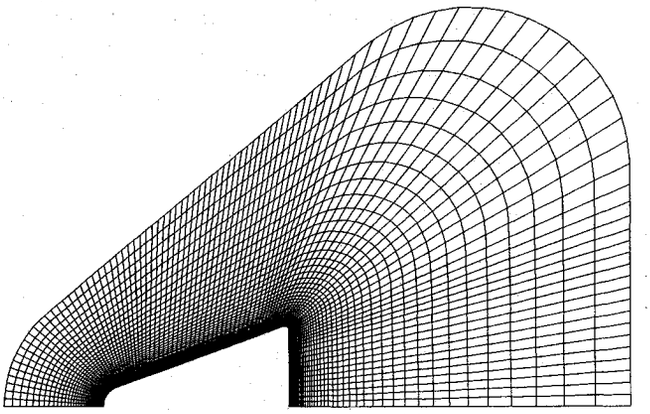

Fig. 1 Computational grid (97 × 65).

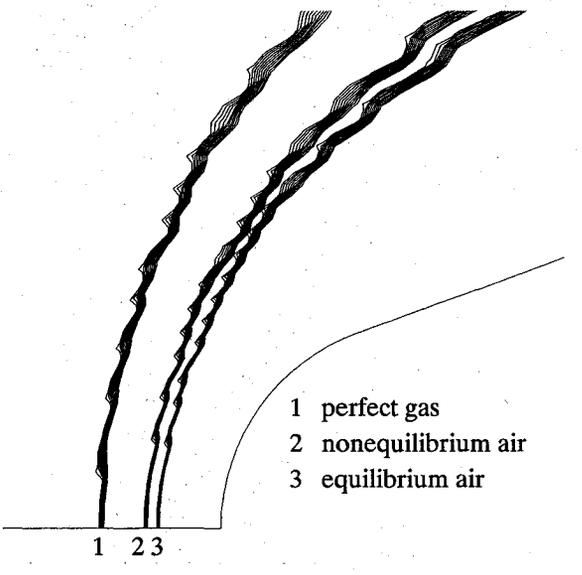

Fig. 2 Shock standoff distance from the wall.

Presented as Paper 92-0641 at the AIAA 30th Aerospace Sciences Meeting, Reno, NV, Jan. 6–9, 1992; received Feb. 3, 1992; revision received Feb. 15, 1993; accepted for publication Feb. 15, 1993.

*Research Assistant, Department of Aeronautical and Astronautical Engineering. Student Member AIAA.
†Associate Professor, Department of Aeronautical and Astronautical Engineering. Associate Fellow AIAA.

prediction of the near-wake flowfield is important for a better understanding of the hypersonic wake.

In hypersonic flight, the high kinetic energy produces a high-temperature flowfield that can dissociate and even ionize the chemical species of the air. Thus, the air is no longer a perfect gas. Chemical reactions take place in the flow, changing species compositions. These chemical phenomena absorb energy, thus decreasing temperature and increasing density. These thermochemical effects can often be integrated into the gasdynamics equations using an equilibrium air model. However, at high altitudes, the chemical state does not reach equilibrium, and a nonequilibrium air model must be employed to match the computational model to the actual flow physics. The objective of the present study is to improve the understanding of the effects of different gas models in hypersonic near-wake calculations.

Physical Modeling

The Navier-Stokes equations are solved in two dimensions to evaluate the effects of different gas models in hypersonic base

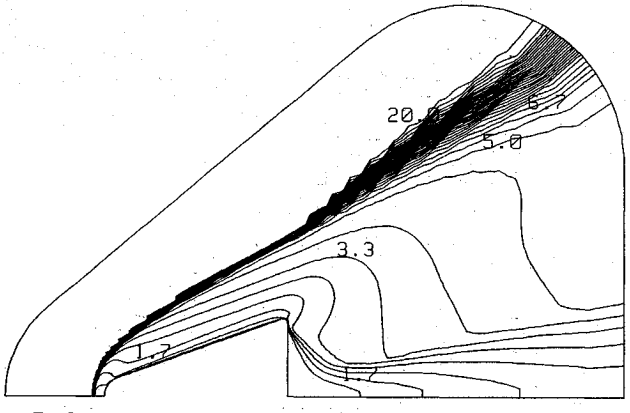

a) Perfect gas

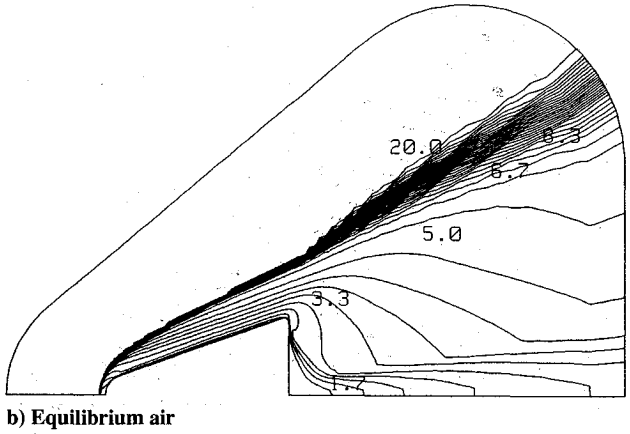

b) Equilibrium air

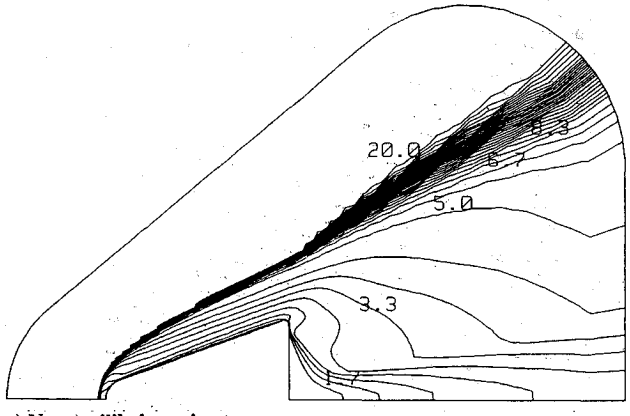

c) Nonequilibrium air

Fig. 3 Mach contours.

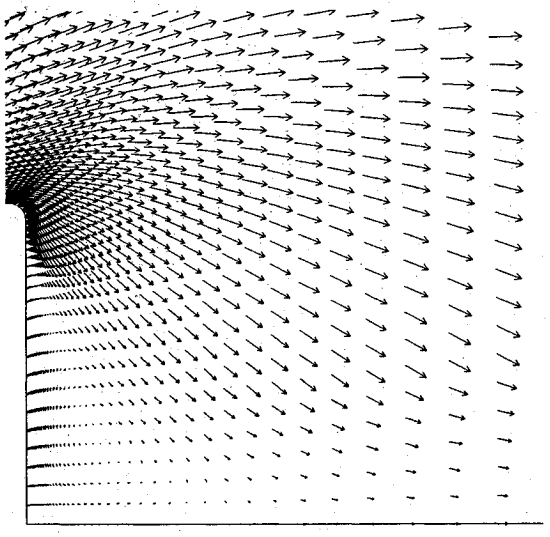

a) Perfect gas

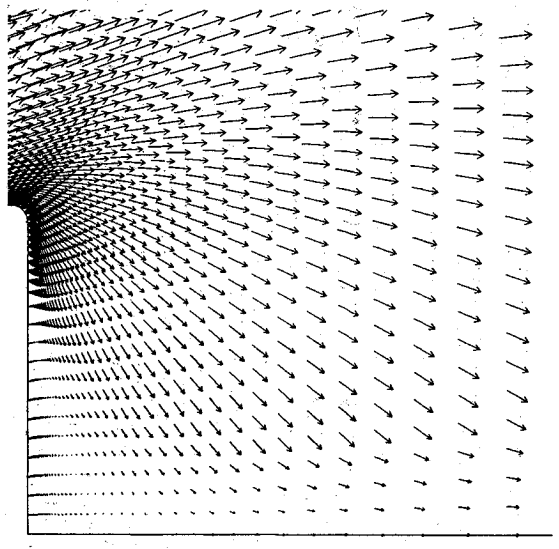

b) Equilibrium air

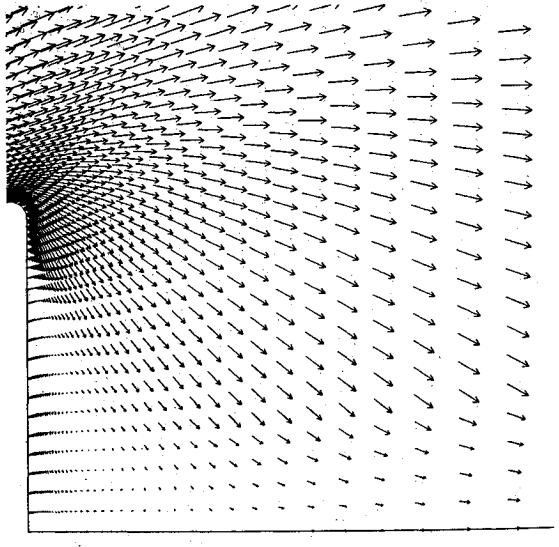

c) Nonequilibrium air

Fig. 4 Velocity profiles near the base.

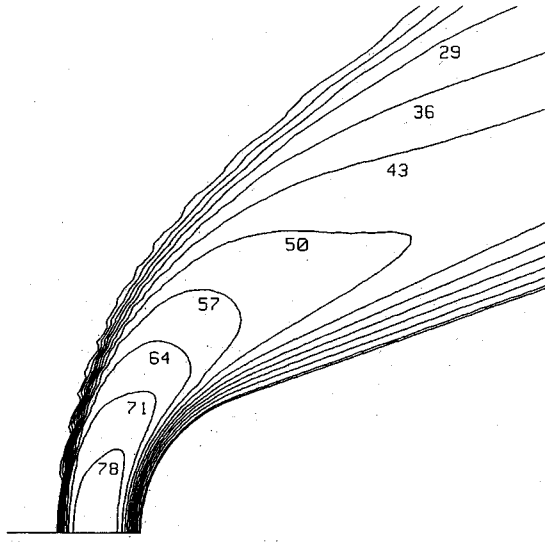

a) Perfect gas (max = 82.4)

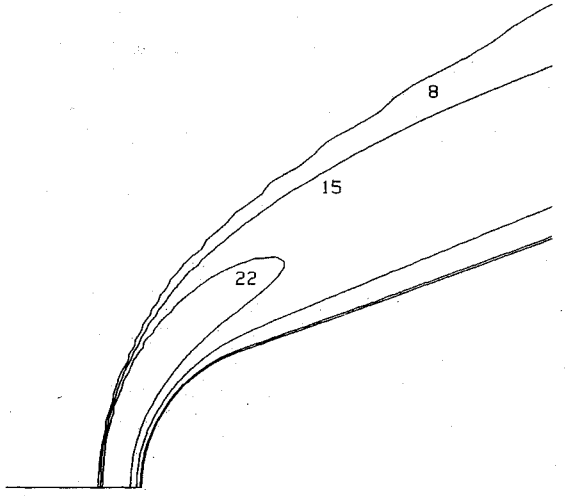

b) Equilibrium air (max = 26.2)

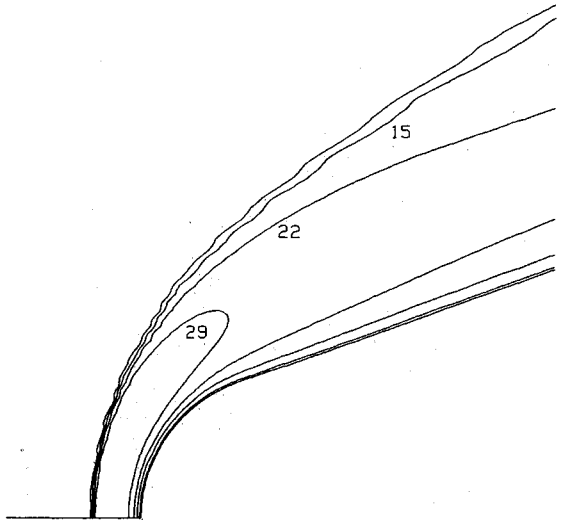

c) Nonequilibrium air (max = 35.7)

Fig. 5 Normalized temperature contours in nose region.

flow calculations. No turbulence model is used, so the flow is assumed to be laminar. Because of the complexity of the base flow, no viscous terms can be ignored as in the thin-layer or parabolized Navier-Stokes equations. Thermochemical effects are modeled with two different approximations: equilibrium air and nonequilibrium air.

In the equilibrium air model, the flow is assumed to be in chemical equilibrium at each point in the flowfield. That is, the time scale for chemical reactions is assumed to be much smaller than the characteristic time scale of the fluid motion. When this is true, all chemical reactions are thought to occur at an infinite rate, and the chemical composition of the air at a point depends only on local thermodynamic properties.

In the nonequilibrium air model, the chemical composition of the air depends on both the thermochemical and fluid dynamic

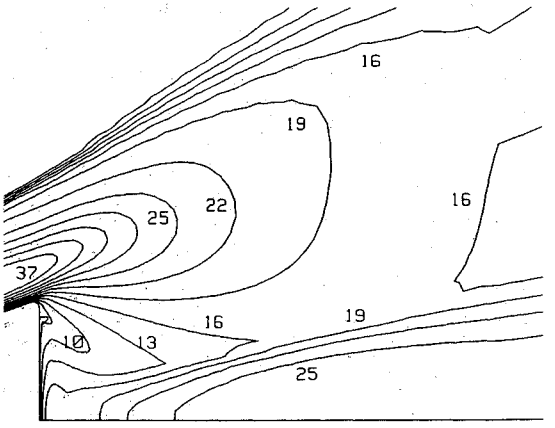

a) Perfect gas

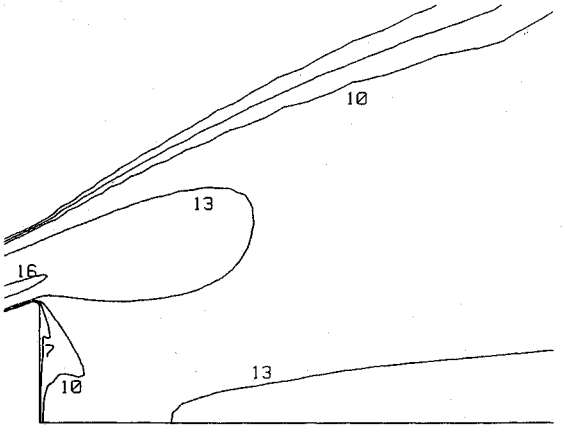

b) Equilibrium air

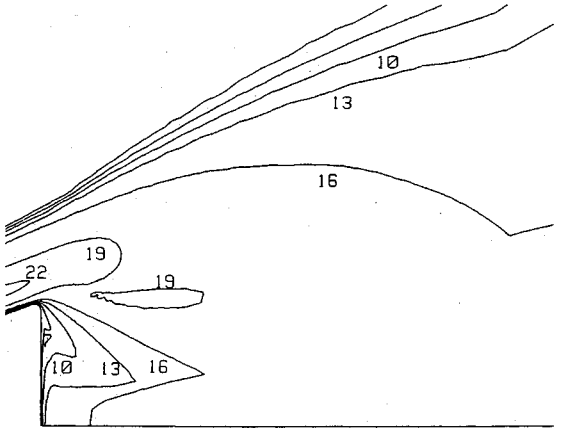

c) Nonequilibrium air

Fig. 6 Normalized temperature contours in base region.

properties of the flow. Conservation equations for each possible species must be solved. These equations balance the time rate of change of the species compositions with convection due to average air motion and production terms due to finite rate chemical reactions. Species diffusion effects[1] can also be included through the use of Fick's law of diffusion; however, they are omitted in the present model for simplicity. In nonequilibrium states, energy is distributed among the translational, rotational, vibrational, and electronic modes. Therefore, multiple temperature definitions[2] may be needed to describe the distribution of energy in different modes. The present model, however, neglects the conservation of vibrational and electronic energy, and a single-temperature model is used.

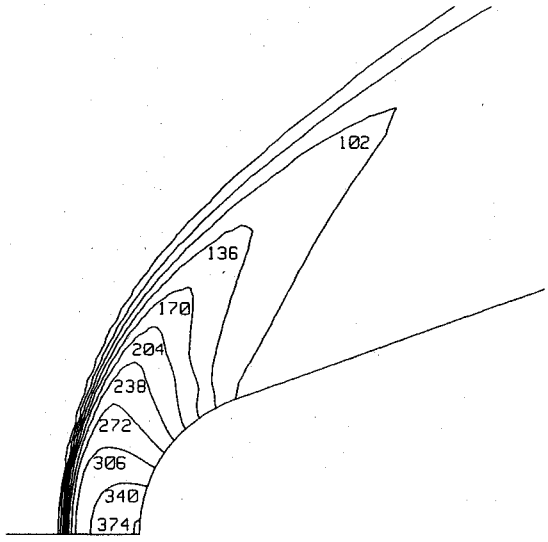

a) Perfect gas (max = 376.1)

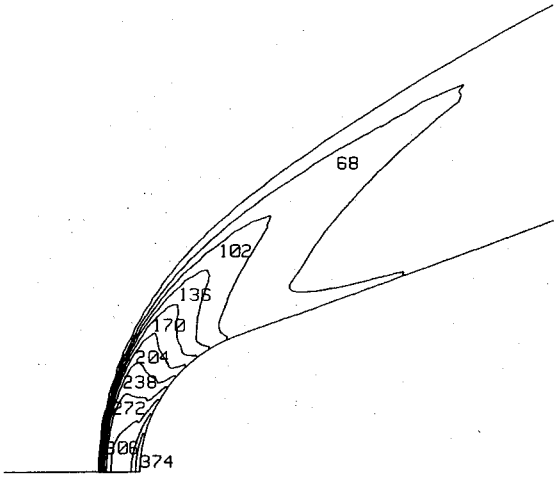

b) Equilibrium air (max = 402.0)

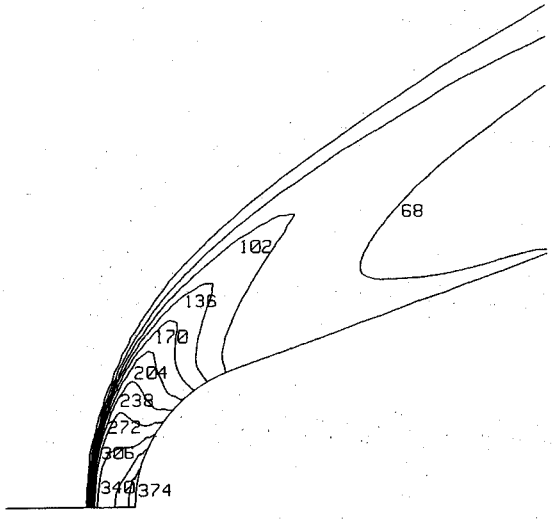

c) Nonequilibrium air (max = 401.6)

Fig. 7 Normalized pressure contours in nose region.

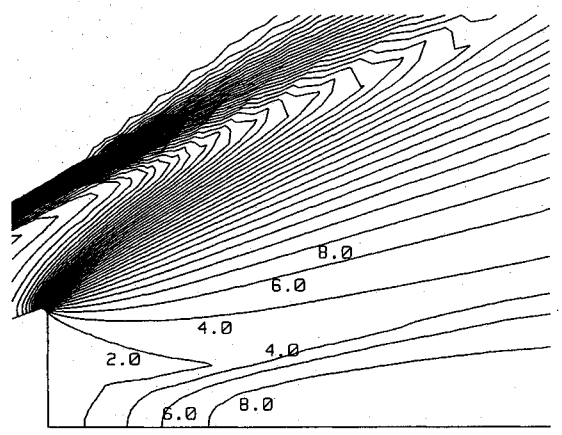

a) Perfect gas

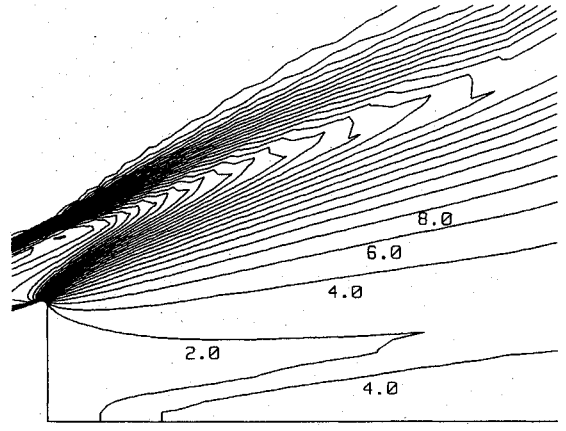

b) Equilibrium air

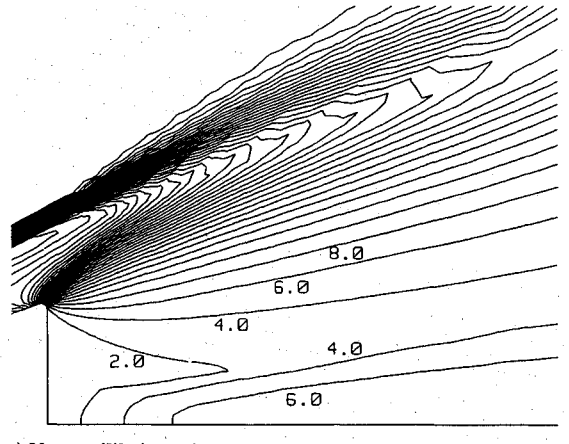

c) Nonequilibrium air

Fig. 8 Normalized pressure contours in base region.

Numerical Methods

A real gas Navier-Stokes code was written for this study. The gasdynamics equations and thermochemical equations are solved using a loosely coupled approach. That is, the gasdynamics equations are solved for a given number of iterations with a fixed chemical composition, and then a chemistry package is called to

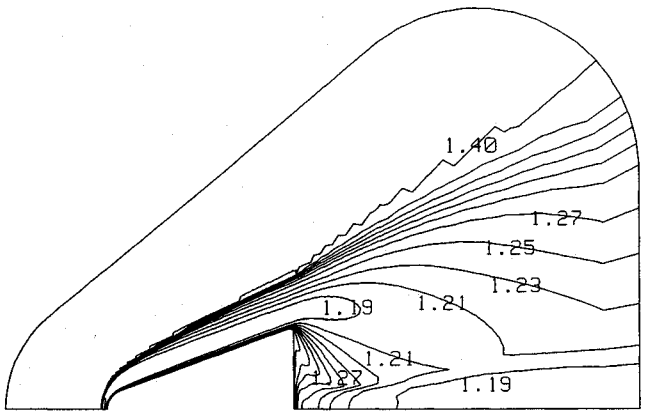

a) Equilibrium air (min = 1.16)

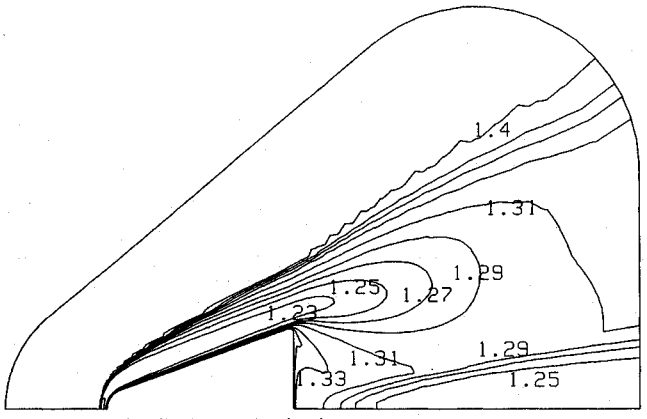

b) Nonequilibrium air (min = 1.21)

Fig. 9 Specific heat ratio contours.

update the species composition and associated thermodynamic properties. Steady-state solutions are obtained as time asymptotes of the unsteady equations.

The system of equations is expressed in curvilinear coordinates to accommodate arbitrary configurations:

$$\frac{\partial Q}{\partial t}+\frac{\partial F}{\partial \xi}+\frac{\partial G}{\partial \eta}=\frac{1}{Re}\left(\frac{\partial F_V}{\partial \xi}+\frac{\partial F_V}{\partial \eta}\right) \tag{1}$$

where

$$Q=\begin{Bmatrix}\rho h\\ \rho uh\\ \rho vh\\ \rho Eh\end{Bmatrix}\quad F=\begin{Bmatrix}\rho Uh\\ \rho uUh+y_\eta p\\ \rho vUh-x_\eta p\\ \rho UHh\end{Bmatrix}\quad G=\begin{Bmatrix}\rho Vh\\ \rho uVh-y_\xi p\\ \rho vVh+x_\xi p\\ \rho VHh\end{Bmatrix}$$

$$F_V=\begin{Bmatrix}0\\ y_\eta\tau_{xx}-x_\eta\tau_{xy}\\ y_\eta\tau_{xy}-x_\eta\tau_{yy}\\ y_\eta f-x_\eta g\end{Bmatrix}\qquad G_V=\begin{Bmatrix}0\\ -y_\xi\tau_{xx}+x_\xi\tau_{xy}\\ -y_\xi\tau_{xy}+x_\xi\tau_{yy}\\ -y_\xi f+x_\xi g\end{Bmatrix}$$

and

$$\tau_{xx}=\mu\left[4\left(u_\xi\xi_x+u_\eta\eta_x\right)-2\left(v_\xi\xi_y+v_\eta\eta_y\right)\right]/3$$

$$\tau_{xy}=\mu\left(u_\xi\xi_y+u_\eta\eta_y+v_\xi\xi_x+v_\eta\eta_x\right)$$

$$\tau_{yy}=\mu\left[-2\left(u_\xi\xi_x+u_\eta\eta_x\right)+4\left(v_\xi\xi_y+v_\eta\eta_y\right)\right]/3$$

$$f=u\tau_{xx}+v\tau_{xy}+\frac{\mu}{(\gamma-1)Pr}\alpha_\xi^2\xi_x+\frac{\mu}{(\gamma-1)Pr}\alpha_\eta^2\eta_x$$

$$g=u\tau_{xy}+v\tau_{xy}+\frac{\mu}{(\gamma-1)Pr}\alpha_\xi^2\xi_y+\frac{\mu}{(\gamma-1)Pr}\alpha_\eta^2\eta_y$$

$$U=u\xi_x+v\xi_y$$

$$V=u\eta_x+v\eta_y$$

The equations are discretized in the conservative form using a finite volume method. The inviscid convective terms are computed using the first-order flux vector splitting of Steger and Warming,[3] and viscous terms are computed using centered differencing. An approximate factorization algorithm[4] is used for time integration. The nonperfect gas models generally destabilize the solution algorithm, reduce the convergence rate, and consequently increase the cost of obtaining a converged solution. Thus, smaller time steps must be used for the nonperfect gas models.

In the equilibrium chemistry model, the species composition of the air is determined through a free energy minimization procedure developed by Gordon and McBride.[5] First, the thermodynamic state is obtained from the fluid dynamics solver, as specified by the values of density and specific internal energy. Then, values of the species concentrations are found that minimize the Helmholtz free energy f at the given thermodynamic state:

$$f=\sum_{s=1}^{n}\mu_s \tag{2}$$

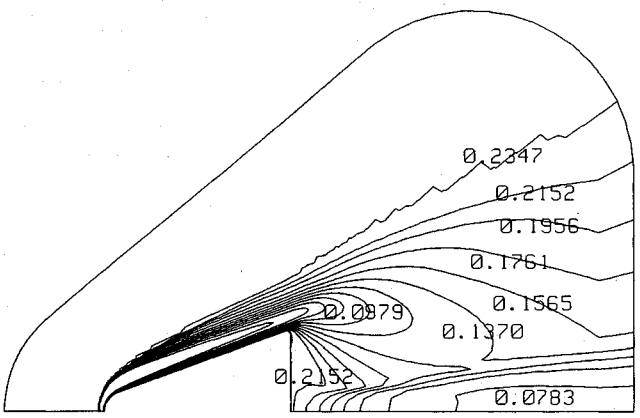

a) Equilibrium air (min = 0.0001)

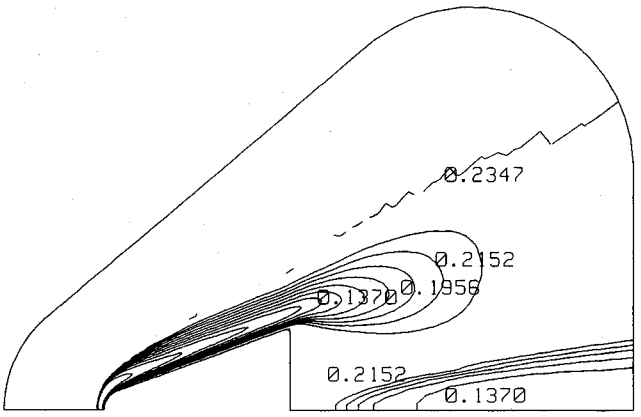

b) Nonequilibrium air (min = 0.0035)

Fig. 10 O_2 concentration.

The Helmholtz free energy is a function of chemical potentials for each species μ_s, which in turn depend on the species compositions and on the temperature and pressure of the mixture. This gives a nonlinear function of species compositions that must be minimized. Constraints are included by using Lagrangian multipliers λ_l, so that the total number of atoms of each species b_l remains conserved. This results in an objective function F, which is to be minimized:

$$F = f + \sum_{l=1}^{m} \lambda_l \left(b_l - b_l^0 \right) \tag{3}$$

where

$$b_l = \sum_{s=1}^{n} \alpha_{ls} \gamma_s$$

Applying the variational condition with respect to γ_s and λ_l to the object function gives a set of nonlinear algebraic equations for the species compositions that are solved using a Newton-Raphson method:

$$\delta F = \sum_{s=1}^{n} \mu_s + \sum_{l=1}^{m} \lambda_l \alpha_{ls} \delta \gamma_s + \sum_{l=1}^{m} \left(b_l - b_l^0 \right) \delta \lambda_l = 0 \tag{4}$$

Once the equilibrium species composition is known, other properties of the mixture, such as specific heats, can be computed from linear sums of species properties. In the present study, eleven chemical species derived from three elements are considered. The elements consist of oxygen, nitrogen, and electrons. The species include the electrically neutral compounds O, O_2, N, N_2, and NO, as well as the ionic compounds O^+, O^-, N^+, N^-, NO^+, and free electron e^-.

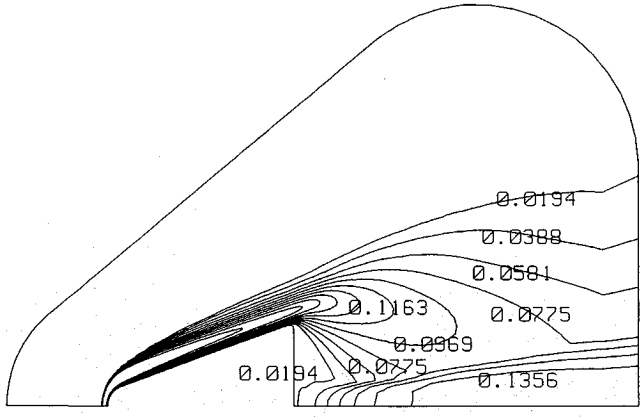

a) Equilibrium air (max = 0.2325)

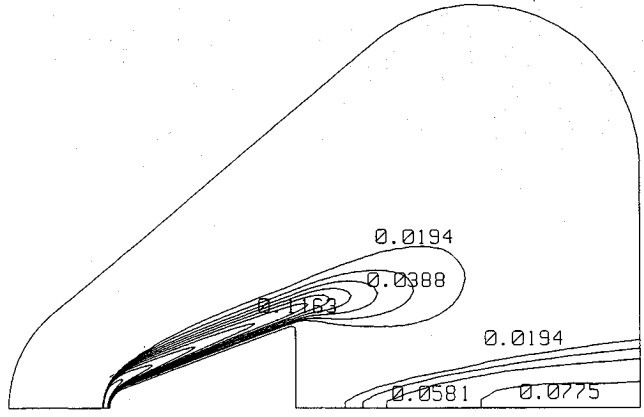

b) Nonequilibrium air (max = 0.2082)

Fig. 11 O concentration.

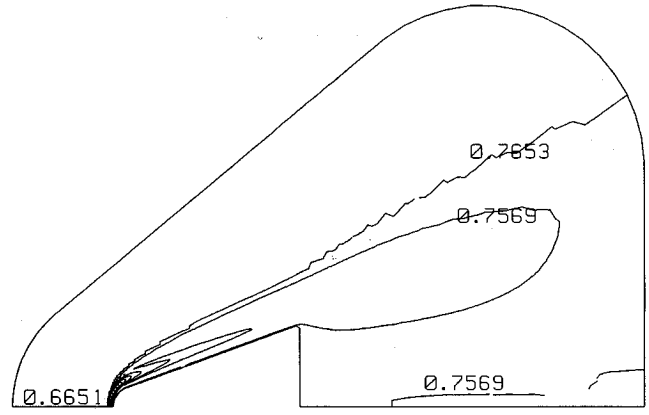

a) Equilibrium air (min = 0.6651)

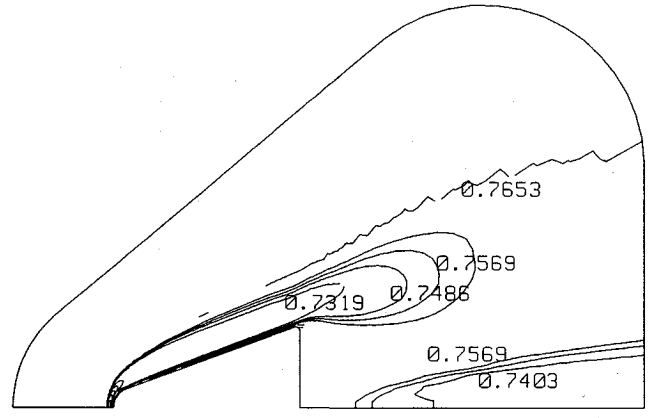

b) Nonequilibrium air (min = 0.6850)

Fig. 12 N_2 concentration.

Coupling the gasdynamics equations with a nonequilibrium air model is much more complicated. The present coupling procedure is derived from the method of Tannehill et al.[1] The procedure begins by estimating the values of pressure, temperature, and enthalpy of the mixture using new values of flow variables from the gasdynamics equations and old species compositions. Species production rates $\tilde{w}_s$ are then calculated as functions of the mixture temperature and the species compositions for all chemical reactions between species:

$$\tilde{w}_s = \tilde{M}_s \sum_{k=1}^{m} \left\{ (\nu''_{k,s} - \nu'_{k,s}) \left[K_{f,k}(\tilde{T}) \prod_{r=1}^{n_t} (\tilde{\rho}\gamma_r)^{\nu'_{k,r}} - K_{b,k}(\tilde{T}) \prod_{r=1}^{n_t} (\tilde{\rho}\gamma_r)^{\nu''_{k,r}} \right] \right\} \tag{5}$$

where γ_r is defined as

$$\gamma_r = \begin{cases} \dfrac{C_r}{\tilde{M}_r} & \text{for} \quad r = 1, 2, \ldots, n \\ \displaystyle\sum_{s=1}^{n} Z_{(r-n),s} \gamma_s & \text{for} \quad r = n+1, n+2, \ldots, n_t \end{cases}$$

The forward and backward reaction rates K_f and K_b are functions of temperature and composition. The tilde represents a

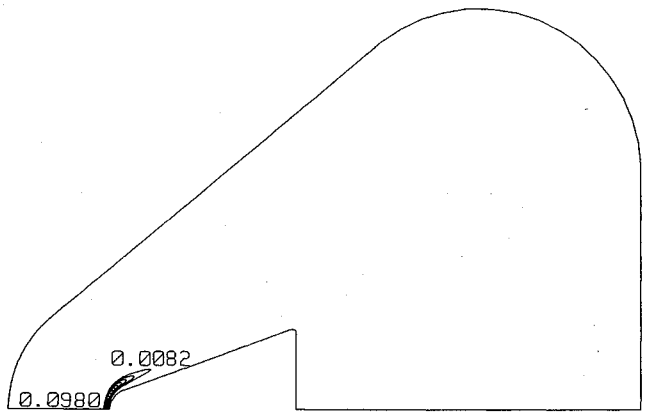

a) Equilibrium air (max = 0.0980)

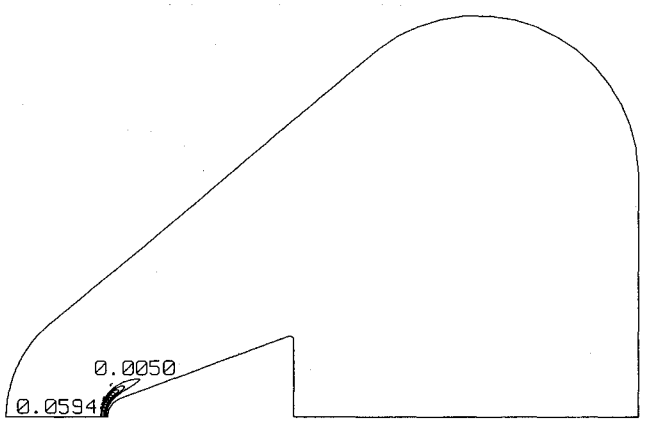

b) Nonequilibrium air (max = 0.0594)

Fig. 13 N concentration.

dimensional quantity. Six reactions are considered between the five neutral compounds O, O_2, N, N_2, and NO. The possibility of ionization is ignored for the nonequilibrium case in this study:

$$\begin{aligned} O_2 + M_1 &\leftrightarrow 2O + M_1 \\ N_2 + M_2 &\leftrightarrow 2N + M_2 \\ N_2 + N &\leftrightarrow 2N + N \\ NO + M_3 &\leftrightarrow N + O + M_3 \\ NO + O &\leftrightarrow O_2 + N \\ N_2 + O &\leftrightarrow NO + N \end{aligned} \tag{6}$$

where M_1, M_2, and M_3 are catalytic third bodies.

The species continuity equations are then integrated for new values of species concentrations with the species production rates as source terms. The nondimensional species continuity equations in curvilinear coordinates are given by

$$\frac{\partial(\rho C_s)}{\partial t} + \frac{\partial(\rho u C_s)}{\partial x} + \frac{\partial(\rho v C_s)}{\partial y} = \dot{w}_s \tag{7}$$

for species s. As in the gasdynamics equations, the species equations are discretized with a first-order Steger and Warming, finite volume method and integrated implicitly using an approximate factorization. Different time scales are used for the fluid motion and the chemical reactions. Smaller time steps are used to overcome the stiffness problem in the chemistry package. Once the species compositions are known, the mixture temperature is estimated from the total energy conservation principle by solving the equation for enthalpy of the mixture $\tilde{h}$ using a Newton-Raphson iteration:

$$\tilde{h} = \sum_{s=1}^{n} C_s \tilde{h}_s \tag{8}$$

The new species compositions and the mixture temperature are used to estimate other mixture properties such as molecular weight, pressure, specific heat ratio, and speed of sound. The chemistry routine is iterated to insure convergence, and the resulting thermodynamic variables are returned to the gasdynamic solver.

Results and Discussions

The effects of different gas models are examined for a two-dimensional, hypersonic flowfield around a blunt-nosed, flat-based projectile. The body has a 20-deg half-angle and a rounded shoulder at the base. Flight conditions are at Mach 20, at an altitude of 73 km where the ambient pressure and temperature are 12.267 P and 196.7 K, respectively. The corresponding Reynolds number is 4.75×10^3 per unit length. The freestream mass fractions are 23.47% oxygen and 76.53% nitrogen. A constant wall temperature of 1000 K is imposed on the body surface. Figure 1 shows the computational grid consisting of 97×65 grid points.

Figures 2 and 3 compare shock standoff distances and Mach number contours for the perfect gas, equilibrium air, and nonequilibrium air models. Differences in shock standoff distance are apparent among the three gas models. The largest shock standoff distance occurs with the perfect gas model, whereas the shortest occurs with the equilibrium air model. Figure 4 compares velocity

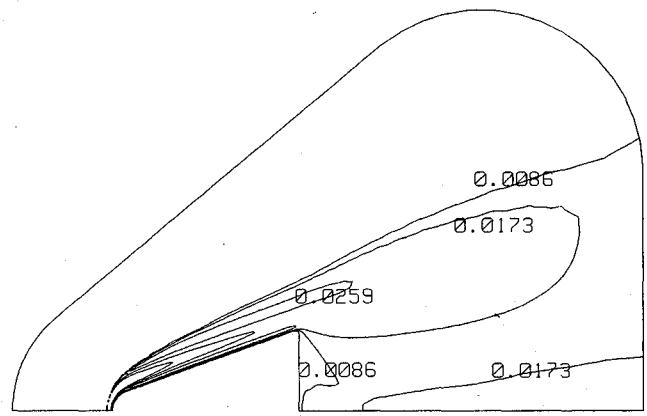

a) Equilibrium air (max = 0.0379)

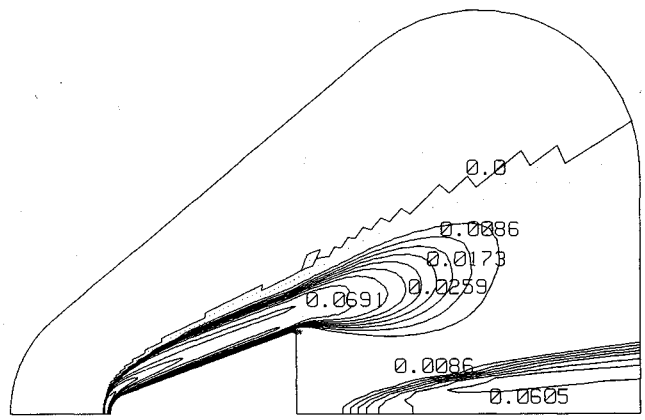

b) Nonequilibrium air (max = 0.1037)

Fig. 14 NO concentration.

profiles near the base. The largest circulation region is formed with the perfect gas model, whereas the smallest is formed with the equilibrium air model. The different gas models also locate the rear stagnation points differently. The farthest rear stagnation point from the base is obtained with perfect gas, whereas the nearest is obtained with an equilibrium air model.

Figures 5 and 6 compare temperature contours in the nose and base regions, respectively. The values in the figure are normalized with respect to the freestream temperature. The different gas models produce very different maximum temperatures in the flow. The temperature immediately behind the bow shock is strongly overpredicted with the perfect gas model at about 16,200 K. It is drastically reduced to 5160 K for the equilibrium model and 7030 K for the nonequilibrium model. The lower temperatures resulting from the nonperfect gas models are attributed to the absorption of energy by the chemical reactions. These differences in shock-layer thickness and maximum temperature affect the downstream flowfield both dynamically and chemically.

Figures 7 and 8 compare pressure contours in the nose and base regions, respectively, for the three gas models. These values are normalized with respect to 1.4 times the freestream value. Pressure is generally less sensitive than temperature to the choice of gas model, because it is a momentum variable and less influenced by the thermodynamic state of the gas. However, the gas model still significantly influences both pressure and temperature in the base flow region.

Distributions of specific heat ratio and species mass concentrations are shown in Figs. 9–14 for the equilibrium and nonequilibrium air models. Near the nose of the vehicle, the different gas models produce differences in the magnitude of thermochemical variables; however, in the base region, major differences are observed in the overall distribution patterns.

Conclusions

The use of different gas models produces significant effects on hypersonic flow calculations. Large reductions in maximum temperature and shock-layer thickness are observed with nonperfect gas models. As expected, the equilibrium air model overpredicts the thermochemical effects compared with the nonequilibrium air model. The differences in maximum temperature and shock-layer thickness influence the downstream flowfield both dynamically and chemically. The gas models produce circulation regions of different sizes and locate the rear stagnation points differently. The gas models strongly affect the thermochemical properties in the base region.

References

[1]Tannehill, J. C., Levalts, J. O., Prabhu, D. K., and Lawrence, S. L., "An Upwind Parabolized Navier-Stokes Code for Chemically Reacting Flows," AIAA Paper 88-2614, June 1988.

[2]Park, C., "Assessment of Two-Temperature Kinetic Model for Ionizing Air,"AIAA Paper 87-1574, June 1987.

[3]Steger, J. L., and Warming, R. F., "Flux Vector Splitting of the Inviscid Gasdynamics Equations with Application to Finite Difference Method," *Journal of Computational Physics*, Vol. 40, No. 2, 1981, pp. 263-293.

[4]Beam, R. M., and Warming, R. F., "An Implicit Factored Scheme for the Compressible Navier-Stokes Equations," *AIAA Journal*, Vol. 16, No. 4, 1978, pp. 393–402.

[5]Gordon, S., and McBride, B. J., "Computer Program for Calculation of Complex Chemical Equilibrium Compositions, Rocket Performance, Incident and Reflected Shocks, and Chapman-Jouguet Detonations," NASA SP-273, March 1976.